POLITECNICO
MILANO 1863

SCUOLA DI INGEGNERIA INDUSTRIALE
E DELL'INFORMAZIONE

Executive Summary of the Thesis

Numerically Efficient Methods for Low-Thrust Collision Avoidance Maneuver Design in Multiple Orbital Regimes

Laurea Magistrale in Space Engineering - Ingegneria Spaziale

Author: Gabriele Dani

Advisor: Prof. Pierluigi Di Lizia

Co-advisors: Prof. Roberto Armellin, PhD Candidate Andrea De Vittori

Academic year: 2021-2022

1. Introduction

The number of artificial materials around the Earth, no longer functional for operative applications, has gradually increased since the start of space activity.
LEO represents the most adopted region for remote sensing, imaging, and commercial applications due to its close proximity to the Earth. The intensive usage of this space sector transforms it into a bullets depository. Furthermore, the proliferation of space junk continues essentially unabated owing to rocket bodies, paint flecks, mission-related payloads, and fragments resulting from previous collisions.
The situation in the GEO ring is widely different because, as far as it is known, the debris spatial density is lower than in some LEO altitudes. The reason relies on the lower number of space missions that interest this region and on the higher distance that gives a higher resident volume. However, the total number of operating objects is overwhelming, and different actions have been taken to cope with this problem at a global level.
Among them, this work focuses on computationally efficient Collision Avoidance Maneuvers (CAMs) in LEO and GEO to make a step forward toward onboard planning. During CAM design, the Probability of Collision (PoC) and the required Δv are minimized. One peculiar aspect of the GEO regime is the satellites slot allocation defined by sharp values of latitude and longitude, also called station-keeping boxes. They must be respected for the entire operative life. For this reason, satellites are forced to frequently perform station-keeping cycles to counteract the perturbation effects on their nominal orbits.
This work initially addresses analytical CAM with a formulation stemmed from [1], by carefully planning the re-enter to the nominal trajectory for the LEO scenario. Bearing in mind that none of the current existing strategies for maneuver execution includes station-keeping, the second part of the research is a procedure capable to solve the EOP associated to SK maneuver including an eventual CAM, still featuring an analytical solution.

2. Fundamentals

This section describes the theoretical background needed to the analytical CAM formulation.

2.1. Conjunction definition

The CAM design process starts considering the short-term encounter between a satellite and debris. The controllable object (in the following called primary object) is described by a state $\mathbf{x}_p = [\mathbf{r}_p; \mathbf{v}_p]$ while debris (secondary object) is identified by the state $\mathbf{x}_s = [\mathbf{r}_s; \mathbf{v}_s]$. In this equations, $\mathbf{r}_i$ and $\mathbf{v}_i$ are the position and the velocity of the centre of mass of the single object measured in a generic reference $\hat{\Re}$.
To compute the collision probability, it is useful to introduce a coordinate system called B-Plane. The origin of this frame lies at the centre of the secondary object at the time of closest approach as depicted in Fig. 1, with the following axes direction:

$$\mathbf{u}_\xi = \frac{\mathbf{v}_p \times \mathbf{v}_s}{||\mathbf{v}_p \times \mathbf{v}_s||}, \ \mathbf{u}_\eta = \frac{\mathbf{v}_p - \mathbf{v}_s}{||\mathbf{v}_p - \mathbf{v}_s||}, \ \mathbf{u}_\zeta = \mathbf{u}_\xi \times \mathbf{u}_\eta \tag{1}$$

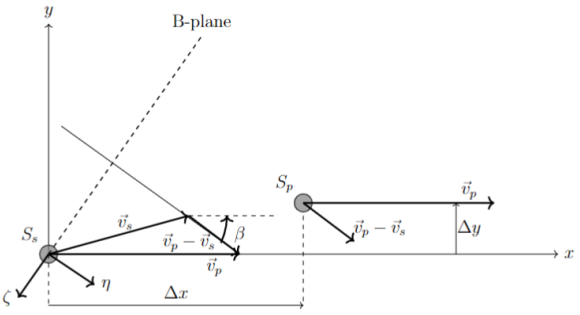

Figure 1: BPlane source [1]

Consequently, the position vector in the B-Plane reference frame is identified as $\mathbf{b}_{3D} = [\xi, \eta, \zeta]^\top$. The rotation matrix to pass from the inertial reference to the B-Plane one is defined as:

$$\mathbf{R}_{b,3D} = [\mathbf{u}_\xi, \mathbf{u}_\eta, \mathbf{u}_\zeta]^\top \tag{2}$$

Additionally, the projection on the η axis is given by:

$$\mathbf{R}_{b,2D} = [\mathbf{u}_\xi, \mathbf{u}_\zeta]^\top \tag{3}$$

Consequently, the 2D position vector in the B-Plane is defined as $\mathbf{b} = [\xi, \zeta]^\top$.

2.2. Chan's PoC model

PoC between the primary and secondary objects experiencing a short-term conjunction can be obtained by integrating the relative position probability density function over a sphere of radius R_A (i.e. the hard body sphere given by the summed primary and secondary radii) at TCA. This assumption is made up for the lack of information about attitude and geometry, especially for the secondary object [2]. Assuming that the relative probability distribution function is Gaussian, an approximated collision probability is obtained with the Chan's method of equivalent cross sectional areas:

$$\mathrm{PoC}(u, v) = e^{-\frac{v}{2}} \sum_{m=0}^{\infty} \frac{v^m}{2^m m!} \left[1 - e^{-\frac{u}{2}} \sum_{k=0}^{m} \frac{u^k}{2^k k!} \right] \tag{4}$$

Where u is the ratio of the impact cross-sectional area to the 1σ B-Plane covariance ellipse area:

$$u = \frac{s_A^2}{\sigma_\xi \sigma_\zeta \sqrt{1 - \rho_{\xi\zeta}^2}} \tag{5}$$

and v is the Squared Mahalanobis Distance (SMD):

$$\begin{aligned} v &= (\mathbf{r}_p - \mathbf{r}_s)^\top \mathbf{R}_{b,2D}^\top \mathbf{C}^{-1} \mathbf{R}_{b,2D} (\mathbf{r}_p - \mathbf{r}_s) = \\ &= \mathbf{b}_p^\top \mathbf{C}^{-1} \mathbf{b}_p \end{aligned} \tag{6}$$

where: $\mathbf{C}$ is the covariance matrix, and $\mathbf{b}_p$ is the primary object position relative to the secondary object in the B-Plane framework.

2.3. Dynamics

The dynamics of space objects in the approximation of a two body encounter can be formulated in terms of the equation of motion:

$$\ddot{\mathbf{r}} = -\frac{\mu}{r^3} \mathbf{r} \tag{7}$$

where $\mathbf{r}$ is the object position in ECI reference. Developing this equation in a state matrix form, and introducing the control acceleration $\mathbf{a}_c$, the two-body dynamics can be rewritten as:

$$\begin{cases} \dot{\mathbf{r}} = \mathbf{v} \\ \dot{\mathbf{v}} = -\dfrac{\mu}{r^3} \mathbf{r} + \mathbf{a}_c \end{cases} \tag{8}$$

This model can be used to implement the CAM in LEO. In the thesis work, the keplerian model is also adopted using as state the classical orbital elements. With reference to the CAM design in GEO, the geopotential perturbation is the major responsible for deviating a satellite from the nominal trajectory. Specifically, the associated

power series is indeed expanded up to the J_{22} term. Therefore, the system dynamics becomes:

$$\begin{cases} \dot{\mathbf{r}} = \mathbf{v} \\ \dot{\mathbf{v}} = -\dfrac{\mu}{r^3}\mathbf{r} + \mathbf{a}_c + \mathbf{a}_{geo} \end{cases} \tag{9}$$

where $\mathbf{a}_{geo} = f(r, \psi, \lambda)$, r is the radial distance, ψ is the geocentric latitude, and λ is the geocentric longitude in polar coordinates (for $\mathbf{a}_{geo}$ see [3]). The previous dynamical model is rerframed using the Equinoctial Orbital Elements (EOE). The mathematical formulation of the linearized dynamics can be seen in [4] and leads to.

$$\dot{\mathbf{x}} = \mathbf{A}(t)\mathbf{x} + \mathbf{D}(t) + \mathbf{B}(t)\mathbf{u} \tag{10}$$

where:

$$\begin{aligned} \mathbf{A}(t) &= \mathbf{A_{kep}}(t) + \mathbf{A_{J2}}(t) \\ \mathbf{D}(t) &= \mathbf{D_{kep}}(t) + \mathbf{D_{J2}}(t) \end{aligned} \tag{11}$$

2.4. State Transition Matrix

Given the non-linear dynamics described in the previous section, the STM labelled as $\mathbf{\Phi}$ allows to map an arbitrary state variation at a certain time t_0 to a final one at t_f according to the following equation:

$$\delta\mathbf{x}_f = \mathbf{\Phi}\delta\mathbf{x}_0 \tag{12}$$

For time-varying systems, $\mathbf{\Phi}(t, t_0)$ can be found by integrating the following equation:

$$\dot{\mathbf{\Phi}}(t, t_0) = \mathbf{A}(t)\mathbf{\Phi}(t, t_0), \ \mathbf{\Phi}(t_0, t_0) = \mathbf{I} \tag{13}$$

where $\mathbf{\Phi}(t_0, t_0)$ is the initial condition and $\mathbf{A}(t)$ is the state matrix obtained by means of a linearization of the dynamical system $\boldsymbol{f}(\mathbf{x}, t)$ around the nominal trajectory $\mathbf{x}_n$:

$$\mathbf{A} = \left.\frac{\partial \boldsymbol{f}(\mathbf{x}, t)}{\partial \mathbf{x}}\right|_{\mathbf{x}_n} \tag{14}$$

3. LEO EOP Design

The LEO design is subdivided in two control strategies. The first is based on cartesian coordinates and fixes the final state after the maneuver. The second one adopts orbital elements and imposes the re-entry at any point of the orbit.

3.1. Point to Point

The main objective of CAMs is to minimize both the PoC and the propellant consumption through the definition of a cost function J:

$$J := \nu\Psi(t_{ca}, \mathbf{x}(t_{ca})) + \int_{t_i}^{t_f} \frac{1}{2}{\mathbf{a_c}}^T\mathbf{a_c}dt \tag{15}$$

where: Ψ represents the interior point equality constraint on the SMD at the time of closest approach (t_{ca}).
Thanks to the Pontryiagin's maximum principle, the optimal control solution can be founded by solving the following Multy Point Boundary Value Problem (MPBVP):

$$\begin{cases} \dot{\mathbf{r}} = \mathbf{v} \\ \dot{\mathbf{v}} = -\dfrac{mu}{r^3}\mathbf{r} - \boldsymbol{\lambda_v} \\ \dot{\boldsymbol{\lambda}}_{\boldsymbol{r}} = \dfrac{\mu}{r^3}\boldsymbol{\lambda_v} - \dfrac{3\mu\mathbf{r}^T\boldsymbol{\lambda_v}}{r^5}\mathbf{r} \\ \dot{\boldsymbol{\lambda}}_{\boldsymbol{v}} = -\boldsymbol{\lambda_r} \end{cases}$$
$$\begin{cases} \mathbf{x}(t_0) = \mathbf{x_0} \\ \mathbf{x}(t_{ca^-}) = \mathbf{x}(t_{ca^+}) \\ \nu\dfrac{\partial\Psi}{\partial\tilde{\mathbf{x}}(t_{ca})} - \boldsymbol{\lambda}^T(t_{ca}^-) + \boldsymbol{\lambda}^T(t_{ca}^+) = 0 \\ \mathbf{x}(t_f) = \mathbf{x_f} \\ \Psi(t_{ca}) = 0 \end{cases} \tag{16}$$

The problem requires to find the initial co-state, λ_{r_0} and λ_{v_0}, and the value of the multiplier ν. In order to perform this operation analytically, It is necessary to approximate the model dynamics through a linearization. This operation is performed thanks to the STM applied on the two trajectory segments interspersed by the TCA. The procedure leads to the expression of the initial co-state as a function of ν. After algebraic operations, the multiplier can be found by solving the fourth-degree equation 17:

$$\begin{aligned} &\nu^2{\mathbf{b_{imp}}}^T\mathbf{Z}^T\mathbf{C}^{-1}\mathbf{Z}\mathbf{b_{imp}} + \\ &\quad - \nu{\mathbf{b_{imp}}}^T[\mathbf{Z}^T\mathbf{C}^{-1} + \mathbf{C}^{-1}\mathbf{Z}]\mathbf{b_{imp}} = \\ &det(\mathbf{I} - \nu\mathbf{U})^2\overline{SMD} - {\mathbf{b_{imp}}}^T\mathbf{C}^{-1}\mathbf{b_{imp}} \end{aligned} \tag{17}$$

All the terms expressed in the Eq.17 can be represented as function of known quantities thanks to the STM.

3.2. Point to Orbit

The procedure adopted is similar to the one described in Sect. 3.1. The objective is to mini-

mize the following functional:

$$J := \nu\Pi(t_{ca}, \mathbf{x}(t_{ca})) + \int_{t_i}^{t_f} \frac{1}{2}\mathbf{a_c}^T\mathbf{a_c}dt \quad (18)$$

where Π represents again the interior point equality constraint on the SMD.
The main difference compared to the previous method lies in the terminal constraints. In fact, to fix the orbit reentry, it is easier to impose five orbital elements, leaving free the final true anomaly.
The Pontryagin's maximum principle leads to the definition of the following Three Point BVP:

$$\begin{cases} \dot{\mathbf{x}} = \mathbf{f}(\mathbf{x}, \mathbf{a_c}) \\ \dot{\boldsymbol{\lambda}} = -\left[\dfrac{\partial \mathbf{f}}{\partial \mathbf{x}}\right]^T \boldsymbol{\lambda} \end{cases}$$
$$\begin{cases} \mathbf{x}(t_0) = \mathbf{x_0} \\ \mathbf{x}(t_{ca^-}) = \mathbf{x}(t_{ca^+}) \\ \nu\dfrac{\partial \Pi}{\partial \tilde{\mathbf{x}}(t_{ca})} - \boldsymbol{\lambda}^T(t_{ca}^-) + \boldsymbol{\lambda}^T(t_{ca}^+) = 0 \\ \mathbf{x}'(t_f) = \mathbf{x_f'} \\ \boldsymbol{\lambda_\theta}(t_f) = 0 \\ \Pi(t_{ca}) = 0 \end{cases} \quad (19)$$

Once again, the problem is to find the initial co-state and the multiplier ν. The procedure is performed like the previous one by adopting the STM to approximate the dynamical model. However, differently from Sect. 3.1, even the interior point constraint leads to a non-linear discontinuity on the co-state variables at TCA. So that, another linearization on the co-state jump has to be performed in order to find an analytical solution.

$$\frac{\partial \Pi}{\partial \mathbf{x}(t_{ca})} = \boldsymbol{\varphi}(\mathbf{x_{ca}}) \approx \boldsymbol{\varphi}(\mathbf{x_{ref}}(t_{ca})) = \boldsymbol{\varphi} \quad (20)$$

The analytical solution can be found by using the second order Taylor's series respect to the nominal point. The result is a second-degree equation where all the terms are defined starting from known quantities.

$$\begin{aligned} &[\mathbf{r_p}(t_{ca}) + \nu\mathbf{Jh} - \mathbf{r_s}(t_{ca})]^T\,\mathbf{Q} \\ &\qquad [\mathbf{r_p}(t_{ca}) + \nu\mathbf{Jh} - \mathbf{r_s}(t_{ca})] = \\ &\overline{SMD} \end{aligned} \quad (21)$$

Once the equation is solved, the value of the multiplier serves for finding the initial co-state.

4. GEO EOP Design

In GEO, due to legal and practical reasons, the spacecraft's position is limited in a window of longitude and latitude. Namely, the target terminal state is chosen by maximizing the resident time in the limit box. The evolution of the spacecraft's location inside the box is governed is mainly driven by the non-spherical Earth harmonics; thus, they are accounted in the dynamical model.
The state variables are represented by the EOE that allows to easily define the target. The final state can be computed with an optimization procedure or analytically, by considering the ballistic motion of the longitude only.
The procedure starts by defining the functional:

$$J := \nu\xi(t_{ca}, \mathbf{x}(t_{ca})) + \int_{t_i}^{t_f} \frac{1}{2}\mathbf{a_c}^T\mathbf{a_c}dt \quad (22)$$

where Π is the interior point equality constraint on the SMD.
Via the Euler Lagrange Equations the linearized state space representation of the MPBVP reads:

$$\begin{cases} \dot{\mathbf{x}} = \mathbf{A}(t)\mathbf{x} - \mathbf{B}(t)\mathbf{B}(t)^T\boldsymbol{\lambda} + \mathbf{D}(t) \\ \dot{\boldsymbol{\lambda}} = -\mathbf{A}(\mathbf{t})^t\boldsymbol{\lambda} \end{cases}$$
$$\begin{cases} \mathbf{x}(t_0) = \mathbf{x_0} \\ \mathbf{x}(t_f) = \mathbf{x_f} \\ \nu\dfrac{\partial \xi}{\partial \mathbf{x}(t_{ca})} - \boldsymbol{\lambda}^T(t_{ca}^-) + \boldsymbol{\lambda}^T(t_{ca}^+) = 0 \\ \xi(t_{ca}) \geq 0 \end{cases} \quad (23)$$

Differently from the CAM provided in LEO, the Maneuver has here the secondary objective to perform the station-keeping re-asset. Therefore, the variation of the state at the TCA is composed by two contributions.

$$\boldsymbol{\delta}\mathbf{x_{ca}} = \boldsymbol{\delta}\mathbf{x_{sk,ca}} + \nu\mathbf{h_{CAM}} \quad (24)$$

If the SK effect is sufficient to respect the PoC constraint, the multiplier value is considered zero and the initial co-state is found by solving a linear system thanks to STM. Otherwise, the procedure follows the approach of Sect. 3.2 by linearizing the discontinuity on the co-state and developing with Taylor's series:

$$\begin{aligned} &[\mathbf{r_p}(t_{ca}) + \nu\mathbf{Jh} - \mathbf{r_s}(t_{ca})]^T\,\mathbf{Q} \\ &\qquad [\mathbf{r_p}(t_{ca}) + \nu\mathbf{Jh} - \mathbf{r_s}(t_{ca})] = \\ &\overline{SMD} \end{aligned} \quad (25)$$

5. FOP Transformation

The FOP transformation binds a fixed acceleration level. The bang-bang bang profile is achieved thanks to a smoothing technique by using hyperbolic tangent.

$$J := \nu\Pi(t_{ca}, \mathbf{x}(t_{ca})) + u_{th} \int_{t_i}^{t_f} a_{max}\epsilon dt \quad (26)$$

where:

$$\epsilon = \frac{1}{2}\left[1 - \tanh\left(\frac{u(\boldsymbol{\lambda}) - u_{th}}{\rho}\right)\right] \quad (27)$$

u_{th} is the switch-on threshold for the thrusters, while ρ is a scaling parameter that governs the transition from continuous to step functions. An iterative procedure changes the value of ρ until matching a discontinuous profile. The algorithm increases the parameter if the solver does not find a solution.

6. Results

6.1. LEO Conjunction

The orbital parameters of the case analyzed in LEO are presented in Tab. 1. The imposed limit on the PoC is 10^{-6}, that corresponds to $SMD = 26.9016$, while the acceleration imposed in the FOP is $a_{max} = 1.5 \cdot 10^{-5}\ \frac{m}{s^2}$.

a[km]	**e**[-]	**i**[deg]	Ω [deg]	$\boldsymbol{\omega}$ [deg]
7186.7	0.00064	98.83	0	289.38

Table 1: Primary object orbital elements.

A grid composed of 15 points for each arc is built. The transfer time spans between 2 and 4 periods. The objects' position in b-plane, Fig. 2 and 3, verify that the algorithm is capable to avoid the collision.

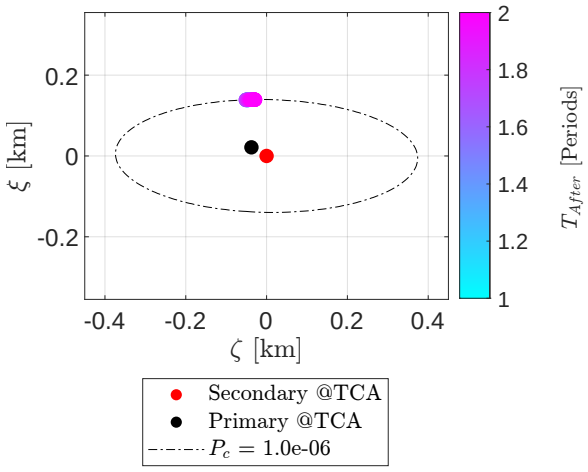

Figure 2: B-plane representation for the EOP PtP solution.

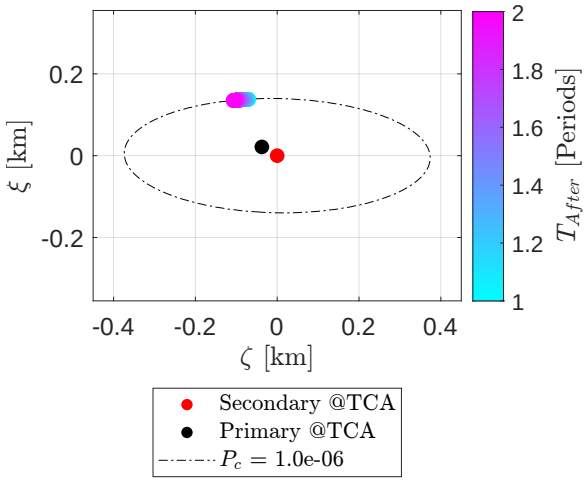

Figure 3: B-plane representation for the EOP PtO solution.

The analytic procedure reports the maneuver costs presented in Fig. 4 and 5

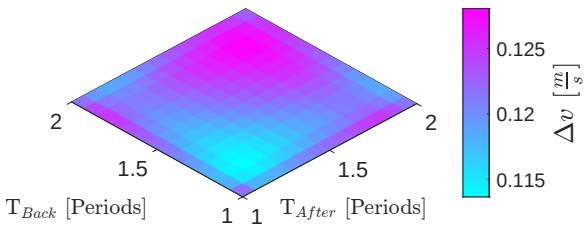

Figure 4: Δv surface for the EOP PtP solution.

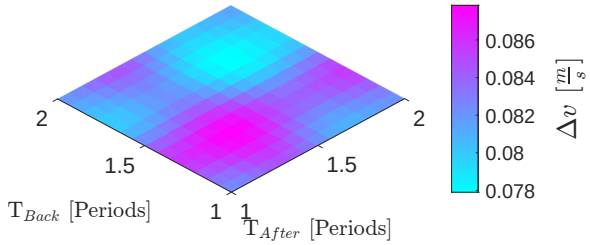

Figure 5: Δv surface for the EOP PtO solution.

The same results are reported for the FOP solutions. Analyzing Fig. 6 and 7 it emerge that the transformation reduce the needed Δv.

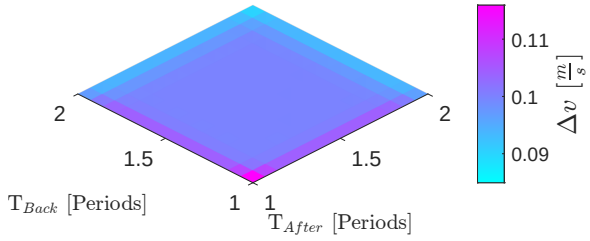

Figure 6: Δv surface for the FOP PtP solution.

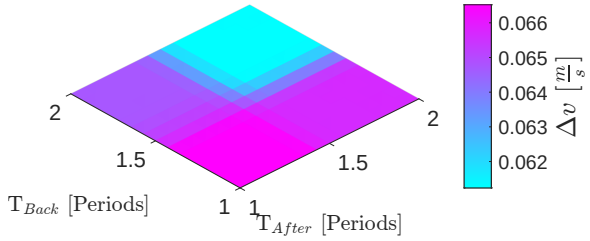

Figure 7: Δv surface for the FOP PtO solution.

The acceleration profiles of the optimal transfers with minimum Δv for PtP and PtO are reported in Fig. 8 and 9.

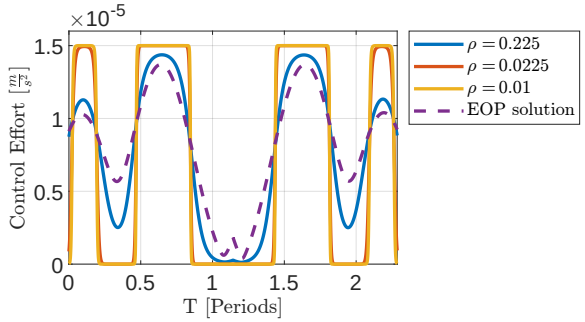

Figure 8: PtP acceleration solution.

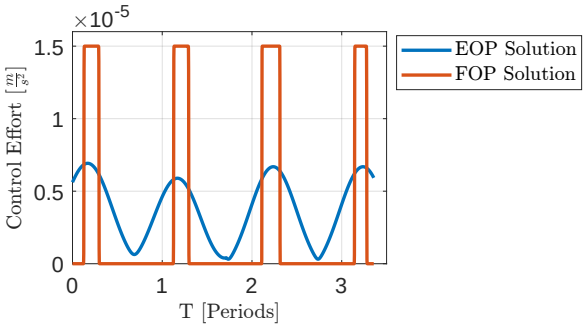

Figure 9: PtO acceleration solution.

6.2. GEO Conjunction

The orbital parameters of the case analyzed in GEO are presented in Tab. 2. The imposed limit on the PoC is 10^{-6}, which corresponds to $SMD = 26.9016$, while the acceleration imposed in the FOP procedure is

a[km]	**e**[-]	**i**[deg]	Ω [deg]	ω [deg]
42220	0	1.55e-4	158.04	315.00

Table 2: Primary object orbital elements.

The initial and final maneuvering points are spaced on a 10 per 10 grid that span between 1.5 to 2 orbital periods.
The Δv required for the EOP and FOP problem is reported in Fig. 10 and 11. It is possible to notice as for certain transfers the FOP results more expensive than the analytic solution. This phenomenon may is be linked to the selected acceleration level and the maneuvering times.

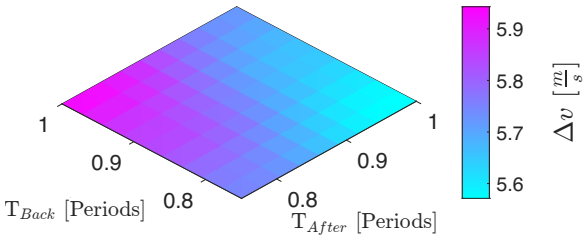

Figure 10: Δv surface for the EOP GEO solution.

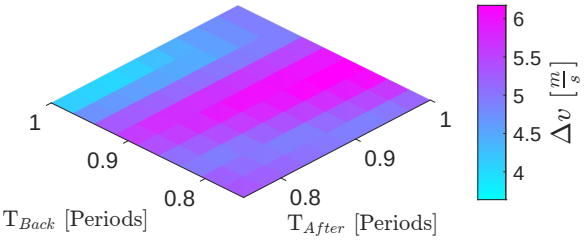

Figure 11: Δv surface for the FOP GEO solution.

The shape of the acceleration required by the optimal solution minimum Δv is reported in Fig 12.

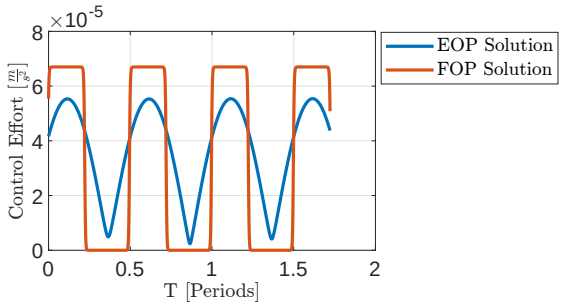

Figure 12: GEO acceleration solution.

In all the cases presented, the perturbation on the original trajectory induced by the station-keeping is sufficient to overcome the limit on the PoC. To verify the effectiveness of the CAM practice, the position of the secondary object at TCA is moved to the one reached by the optimal transfer. Fig. 13 shows that the algorithm is capable to modify the trajectory to reach the SMD limit.

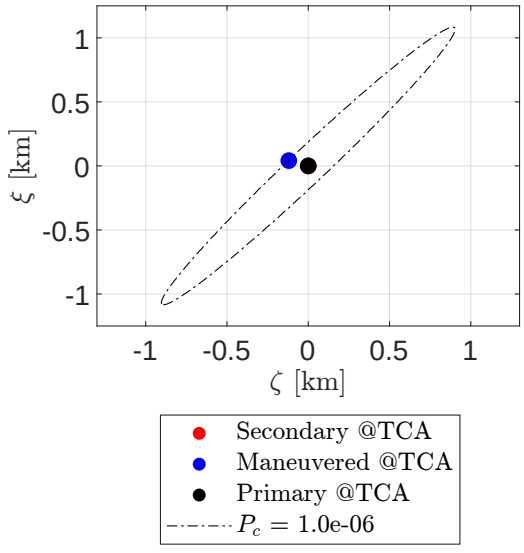

Figure 13: B-plane CAM GEO.

7. Conclusions

The strategies developed here represent the improvement of the already existing collision avoidance techniques. The introduction of a dynamical model based on orbital elements was a crucial aspect to analyze the problem from a different perspective. It allows reducing the problem complexity leading to an easier formulation of the operative constraints opening new borders on the application of collision avoidance practices. Analyzing the obtained results, the required Δv is compatible with low-thrust propulsion as long as the maneuver is executed far enough from conjunction. Moreover, the MPBVP strategy allows to combine CAM with station-keeping, executing the latter only if it is enough for satisfying the SMD constraint at TCA. In all the cases, the computational time required for the maneuver design is always in the order of few seconds, which is deemed to be acceptable for the onboard execution.

8. Acknowledgements

I would like to express my deepest gratitude to my advisor Professor Pierluigi Di Lizia, for having made this work possible, and my co-advisors Professor Roberto Armellin and PhD Candidate Andrea De Vittori for their precious support and wise advice. A special thanks goes to GMV, that provided me the information relative to the conjunction in GEO.

References

[1] M. F. Palermo, "Numerically efficient methods for impulsive and low-thrust collision avoidance manoeuvre design," Master's thesis, School of industrial and information engineering, Department of aerospace science and technology, Politecnico di Milano, Italy, 2021.

[2] J. Hernando-Ayuso and C. Bombardelli, "Low-thrust collision avoidance in circular orbits," *Journal of Guidance, Control, and Dynamics*, vol. 44, pp. 983–995, May 2021.

[3] L. LI, I. Gkolias, C. Colombo, and J. Zhang, "Design of low-thrust control in the geostationary region for station keeping," 2019.

[4] C. Gazzino, "Dynamics of a Geostationary Satellite," Nov. 2017.